2021-06-11

Experimental Analysis and Material Characterization of Ultra High Temperature Composites

Ghoshal, Anindya; Walock, Michael J.; Nieto, Andy; Murugan, Muthuvel; Hofmeister-Mock, Clara; Pepi, Marc; Bravo, Luis; Wright, Andrew; Luo, Jian

ASME

Ghoshal, A., Walock, M. J., Nieto, A., Murugan, M., Hofmeister-Mock, C., Pepi, M., ... & Luo, J. (2021, June). Experimental Analysis and Material Characterization of Ultra High Temperature Composites. In Turbo Expo: Power for Land, Sea, and Air (Vol. 84997, p. V006T02A010). American Society of Mechanical Engineers.
http://hdl.handle.net/10945/68554

Proceedings of ASME Turbo Expo 2021
Turbomachinery Technical Conference and Exposition
GT2021
June 7-11, 2021, Virtual, Online

GT2021-60384

Experimental Analysis and Material Characterization of Ultra High Temperature Composites

Dr. Anindya Ghoshal[1], Dr. Michael J. Walock[1], Dr. Andy Nieto[2], Dr. Muthuvel Murugan[1], Dr. Clara Hofmeister-Mock[1], Mr. Marc Pepi[1], Dr. Luis Bravo[1], Mr. Andrew Wright[3], and Prof Jian Luo[3]

[1]U.S. Army Research Laboratory, Aberdeen Proving Ground, Maryland
[2] Naval Postgraduate School, Monterey, California
[3]University of California, San Diego, California

ABSTRACT

Ultra high temperature ceramic (UHTC) materials have attracted attention for hypersonic applications. Currently there is significant interest in possible gas turbine engine applications of UHTC composites as well. However, many of these materials, such as hafnium carbide, zirconium carbide, and zirconium diboride, have significant oxidation resistance and toughness limitations. In addition, these materials are very difficult to manufacture because of their high melting points. In many cases, SiC powder is incorporated into UHTCs to aid in processing and to enhance fracture toughness. This can also improve the materials' oxidation resistance at moderately high temperatures due to a crack-healing borosilicate phase. ZrB_2-SiC composites show very good oxidation resistance up to 1700 °C, due to the formation of SiO_2 and ZrO_2 scales in numerous prior studies. While this may limit its application to hypersonic applications (due to reduced thermal conductivity and oxidation resistance at higher temperatures), these UHTC-SiC composites may find applications in turbomachinery, as either stand-alone parts or as a component in a multi-layer system.

The US Army Research Laboratory (ARL), the Naval Postgraduate School (NPS), and the University of California – San Diego (UCSD) are developing tough UHTC composites with high durability and oxidation resistance. For this paper, UHTC-SiC composites and high-entropy fluorite oxides were developed using planetary and high-energy ball milling and consolidated using spark plasma sintering. These materials were evaluated for their oxidation-resistance, ablation-resistance, and thermal cycling behavior under a DoD/OSD-funded Laboratory University Collaborative Initiative (LUCI) Fellowship and DoD Vannevar Bush Fellowship Program. In the present paper experimental results and post-test material characterization of SPS sintered ZrB_2, ZrB_2+SiC, ZrB_2+SiC+HfC, HfC+SiC, and HfC+ZrB_2 pellets subjected to ablation test are presented.

NOMENCLATURE

ARL = U.S. Army Research Laboratory
CTE = Coefficient of Thermal Expansion
DEVCOM = US Army Combat Capabilities Development Command
DoD= Department of Defense
GGT= Gas Generator Turbine
GTE = Gas Turbine Engines
HEO= High Entropy Oxides
LUCI= Laboratory University Collaborative Initiative
NPS =Naval Postgraduate School
TBC = Thermal Barrier Coatings
UCSD=University of California, San Diego
UHTCs = Ultra High Temperature Composites

INTRODUCTION

To meet the demands of current and future requirements, military gas turbine engines (GTEs) are required to operate at much higher temperatures for improved power-density and efficiency. Current engine temperatures can exceed 1500 °C, with future Brayton cycle engines projected to exceed 2000 °C to meet the higher power requirements. Currently, monolithic metallic components, with good high temperature tolerance, creep strength, and fracture toughness have been cost-effective solutions. Intermetallics and single-crystal materials, such as nickel-based and molybdenum-base superalloys have improved thermomechanical fatigue, with higher melting points and lower coefficients of thermal expansion (CTE), as compared to monolithics. In addition, thermal barrier coatings (TBCs), in conjunction with bleed-air from advanced cooling hole geometries, are used to protect the underlying substrate materials from the extreme temperatures within GTEs. Most of the SiC-SiC (Silicon carbide) ceramic matrix composite (CMC) materials are envisioned for hot section components including stator vanes, rotor blades, shroud, turbine disk, combustor liner and baffles, and augmentor components. The Ox-Ox (typically aluminum oxide) CMC materials are used or envisioned for use in exhaust nozzles, engine centerbody, engine nacelles, intake fan, compressor and diffuser components. However while current advanced engines reach turbine inlet temperatures of >1700 °C, future Brayton cycle engines will require materials

that can sustain >2000 °C. Current state of the art SiC-SiC CMCs even with T/EBCs and bleed air will not be able to sustain those temperatures. Figure 1 illustrates the historical evolution of high temperature propulsion materials and DEVCOM ARL's vision of the **Generation Next** materials [1-2]. UHTCs could be incorporated as either layers within a multi-layer system, or as a constituent in a ceramic system with a tailored functional gradient.

Figure 1: Evolution of High Temperature Materials for Propulsion Applications

For hypersonic applications the materials requirements for expendable engines and thermal protection systems similarly exceed 2000 °C [3-9]. This has motivated a tremendous explosion in high-temperature materials research. The rapid transition of the recently discovered advanced high entropy metal diborides and oxide fluorites ceramics to hypersonic systems programs will significantly revolutionize the operation capabilities of current hypersonic technology development programs. For hypersonic applications that exist outside the atmosphere, oxidation is not a large issue because of the lack of oxygen, but for hypersonic applications that remain within the atmosphere, as with GTE applications, oxidation must be taken into account. UHTCs with stable high temperature oxides such as HfO_2, Ta_2O_5, and ZrO_2 are particularly promising.

In the case of reusable vehicles/engines operating at sustained conditions at 2000 °C or higher, revolutionary non-ablative materials such as Ultra High Temperature Ceramics (UHTC) are needed. Here high thermal-conductive ceramics that can withstand such high temperatures are considered, where the heat is conducted and radiated away from leading edges or other hot spots. In this context, a limited number of refractory borides (UHTCs), for example, ZrB_2 possess a unique combination of these important properties. UHTCs possess much higher thermal conductivity than conventional engineering ceramics such as Si_3N_4 or Al_2O_3. However, there are still several challenges relating to reinforcement of the mechanical properties, rapid oxidation at high temperatures, as well as difficulties in manufacturing that need to be addressed.

Addressing high temperature propulsion material challenges, requires the development of atomistic and thermodynamic frameworks capable of modeling the material behavior and predicting system response under the complex hydrodynamic loading, transport kinetics, and corrosion. The material high operating temperature requires modeling the effects of oxidation, thermo-mechanical damage and degradation. Oxidation is a well-known bottleneck in the development of high temperature materials for aero-propulsion (GTE engines) and hypersonic flight applications. The oxide scale is subject to complex mechanical (shear flow and vapor pressure) and high temperature conditions. While various materials selections have been investigated experimentally, basic understanding of oxygen transport through the complex oxide scale microstructure of UHTC remains elusive. UHTCs are characterized by melting temperatures in excess of 3000 °C and have structural, physical, transport and thermodynamic properties suitable for use as thermal barriers in extreme environments [3-9].

Ultra-High Temperature Ceramic Composites

Ultra-high-temperature ceramics (UHTCs), a series of covalently bonded borides, carbides and nitrides including TaC, ZrB_2, ZrC, HfB_2, HfC and HfN, have very high melting temperatures, chemical stability, electrical and thermal conductivities and resistance to corrosion. Current ultra-high temperature ceramic materials experience challenges relative to thermal shock, oxidation, toughness and manufacturing. These issues severely restrict operational capabilities of hypersonic systems (missiles and glide vehicles). UHTC composites based on HfC, ZrB_2 and SiC are designed to overcome these challenged and are explored for potential GTE applications in this paper. UHTCs have melting temperatures of up to 3900 °C that may revolutionize the temperature envelope for high temperature materials [Figure 2] [6]. UHTCs have attracted attention for hypersonic applications and UHTC composites applications in turbomachinery will allow a higher operational temperature at the GGT. In general the UHTC has demonstrated excellent oxidation resistance, high temperature strength. This paper will present the results of the testing and microstructure characterization of the developed composite UHTCs. ARL is also studying high entropy ceramics including five solid solution systems of fluorite oxides and borides [10-11].

While UHTCs have attracted attention for hypersonic applications, it is envisioned by the authors that UHTC composites are the next generation of materials for GTE applications as the composite approach enables higher oxidation resistance and high temperature strength. Hafnium is a transition metal[19-23] which is a good absorber of neutrons and is used in control rods of nuclear reactors [20]. Hafnium Carbide (HfC) has one of the highest known melting point [Figure 2] with an oxide that is stable up to 2200 °C. ZrB_2-SiC shows good oxidation resistance up to 1700 °C. SiC enables higher densification by provide a high flux phase that readily diffuses. The dual phase microstructure exhibits higher toughness as cracks experience dissimilar interfaces. SiC enhanced oxidation resistance through the formation of protective SiO_2 and ZrO_2 layers.

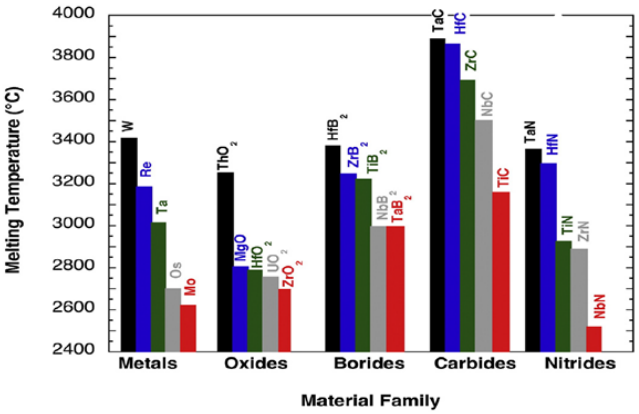

Fig. 2. UHTC material family [6]

Thermochemistry of ZrB_2 and HfC UHTC compositions

Zirconium diboride (ZrB_2) ceramics have relatively low oxidation resistance and fracture toughness without the addition of a secondary reinforcement phase or sintering aid [12-18]. When exposed to moderately high temperatures, ZrB_2 readily oxidizes, as shown in Equation 1[3].

$$ZrB_2\ (cr) + \frac{5}{2}O_2(g) \rightarrow ZrO_2(cr) + B_2O_3(l) \quad (1)$$

At temperatures below 1100°C, B_2O_3 forms a continuous layer. At temperatures between 1100°C to 1400°C, volatilization of B_2O_3 phase commences. At temperatures above 1400°C, B_2O_3 volatizes at a rate faster than it is produced, leaving behind only the non-protective, porous ZrO_2 scale. Such degradation can cause connected open porosity as outgassing to the surface occurs. In addition, boria phase no longer seals grain boundaries or formed cracks, leading to significant degradation of high temperature oxidation resistance and strength. Therefore, for practical use at temperatures above 1100°C, additives such as silicon carbide (SiC), which also serves as a sintering aid, assists in increasing oxidation resistance and toughness of the material by forming a protective borosilicate glass layer [16]. As the boria does at lower temperature, the borosilicate glass seals cracks, effectively healing them and inhibiting further intrusion of oxygen [Figure 3]. The layer of borosilicate glass in ZrB_2-SiC material substantially decreases the original oxidation rate of ZrB_2 above temperatures of 1200°C and prevents the further erosion of internal material. Because SiO_2 has a lower volatility than B_2O_3, the ZrB_2-SiC material shows a slower, diffusion-controlled mass gain, Equation 2 [12,16].

$$\alpha SiC\ (cr) + \frac{3}{2}O_2(g) \rightarrow SiO_2(l) + CO(g) \quad (2)$$

The SiO_2 scale layer remains protective until at least 1500°C [12]. In an air environment from 1500°C-1800°C, the surface of ZrB_2-SiC has a layered structure characterized by an outer, oxidized layer that is silica-rich and demonstrates passive oxidation behavior at a much higher temperature range than monolithic ZrB_2. Under the oxidized layer, research has showed there is a subscale of crystalline zirconia with little silicate, then a SiC-depleted region consisting of ZrB_2 or ZrO_2 followed by the unaffected base material [12,13]. Figure 3 depicts the layer formation as a specimen is heated.

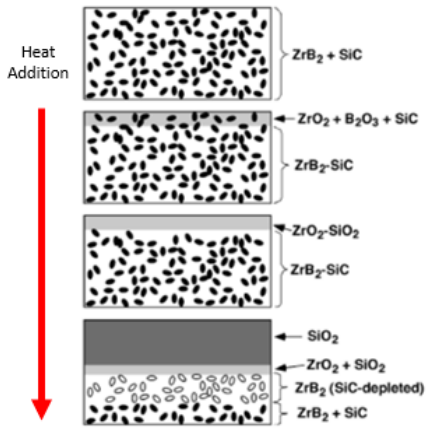

Figure 3: Reaction Sequence for Formation of protective oxide scales in a ZrB_2-SiC Sample heated to 1500°C. Adapted from [16].

The direct sublimation of SiC also becomes possible as shown in Equation 3, which partially accounts for the SiC-depleted areas [12].

$$SiC\ +\ O_2(g) \rightarrow SiO\ (g) + CO(g) \quad (3)$$

At lower temperatures, silicon carbide (SiC) additions to hafnium carbide have had the effect of reducing pores and improving oxidation resistance [22]. For this reason, HfC-SiC is being researched for its potential to reduce oxidation at temperatures around and above 2000 °C. At high temperatures, HfC oxidizes into HfO_2 according to Equation 4 and SiC oxidizes into SiO_2 or SiO according to Equation 5 and Equation 6 [22].

$$HfC + 2O_2 \rightarrow HfO_2 + CO_2 \quad (4)$$
$$SiC + 2O_2 \rightarrow SiO_2 + CO_2 \quad (5)$$
$$SiC + O_2 \rightarrow SiO + CO \quad (6)$$

The presence of water vapor in contact with SiO_2 is known to lead to recession, and underscores the need to test UHTCs in realistic combustion flows to assess the degree of water vapor attack at the small scales at which SiO_2 forms in UHTCs. It is very likely UHTCs may need an environmental barrier coating such as Yb-disilicate layer which is used for SiC-SiC CMCs to form a water vapor barrier to prevent this recession. HfC has a melting temperature of 3890 °C [5]. HfO_2 has a melting temperature of 2810 °C [5]. SiO_2 has a melting temperature of 1710 °C [23]. Because of this, at extremely high temperatures, SiO_2 is in liquid form. This liquid phase can flow both outward and inward into pores [4]. Previous research has shown that at temperatures above 2500 °C, HfO_2 granules become suspended in melted SiO/SiO_2. This research showed that the melted SiO/SiO_2 partially prevented the flow of gases through the oxide layer, improving the oxidation resistance of the material, which could also prove advantageous for preventing ingress of water vapor. However, the oxide layer also became severely degraded at the high temperatures [22].

EXPERIMENTAL SETUP AND MATERIALS

Starting Materials

In this research work the acquired UHTC powder included Silicon Carbide (SiC), Hafnium Carbide (HfC) and Zirconium Diboride (ZrB_2). Table 1 gives the details of the powders procured. The UHTC composites tested in the paper were synthesized using this starting materials. Composite samples included HfC (H1), HfC-30 vol.% SiC (H2), ZrB_2-20 vol.% SiC (ZS1), ZrB_2-30 vol.% SiC (ZS2), and ZrB_2-25 vol.% SiC-5 vol.% HfC (ZS3).

Figure 4 left image shows SiC powder as received and the right one shows the powder under higher magnification. A fine particulate size was used to aid in effective packing in the composite mixture and to aid sintering. No stand-alone SiC pucks are consolidated as SiC is known to lack the necessary oxidation and high strength mechanical properties at temperature > 1500 °C.

Spark Plasma Sintering Processing of UHTC Composites

ZrB_2, SiC and HfC based composite powders are processed using spark plasma sintering (SPS) parameters, with time, pressure, and temperature being the primary processing variables. This was performed at University of California, San Diego NanoEngineering Lab facility. For the ZrB_2 based composites, the temperature increased at 200°C/min for 8 minutes until reaching 1625°C while pressure increased from a rate of 10 MPa to 70 MPa over 3 minutes. Next, with pressure held at 70 MPa, temperature increased at 58.3°C/min until reaching 1800°C. This temperature and pressure, 1800°C and 70 MPa, was held for 10 minutes. After 21 minutes, current is turned off and pressure released at 70 MPa/min. The specimen is cooled under vacuum until below 500°C. For the HfC materials, the process was modified so that the peak temperature was 1950 °C. Figure 5 depicts SPS schedule for ZS1, ZS2, and ZS3 specimens. Figure 6 depicts SPS processing schedule for temperature and pressure for H1 and H2 specimens. Each sample was fabricated as 1 inch disks and 4-5 millimeter thickness.

Powder	Vendor	Particle Size	Quantity	Product Number
Hafnium Carbide (HfC)	ALB Materials Inc	APS: 0.8 µm	500 g	Micro-HfC-0.8
Zirconium Diboride (ZrB_2)	HC Starck	90% < 6 µm APS (d_{50}): 1.5 – 3.0 µm	1 kg	ZrB2 Grade B (AB 146811)
Silicon Carbide (SiC)	HC Starck	APS (d_{50}): 0.5 µm	1 kg	SiC Grade BF 17 (AB 147382)

Table 1: UHTC powders used for this research at ARL

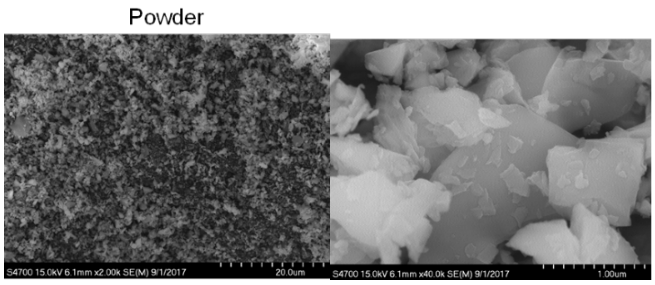

Figure 4: Left image shows SiC powder as received and the right one shows the powder under higher magnification.

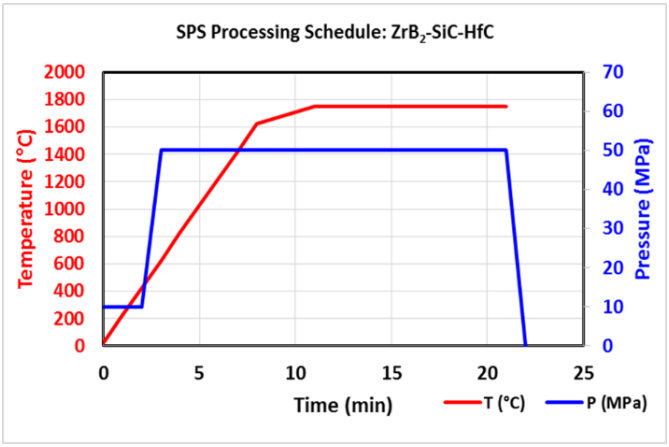

Figure 5: SPS Fabrication template of ZrB_2 based UHTC composites samples

Figure 7 shows the starting HfC powder and the subsequent HfC after it was consolidated using SPS. The consolidated microstructure is shown in the right hand side of Figure 5.

The ZrB_2 powder has been used to develop ZrB_2-SiC and ZrB_2-HfC-SiC composites. Figure 8 shows the ZrB_2 as received powder micrographs and Figure 9 shows the consolidated ZrB_2-SiC and ZrB_2-HfC-SiC composites micrographs. Figure 10 illustrates the consolidated HfC-SiC composite micrographs.

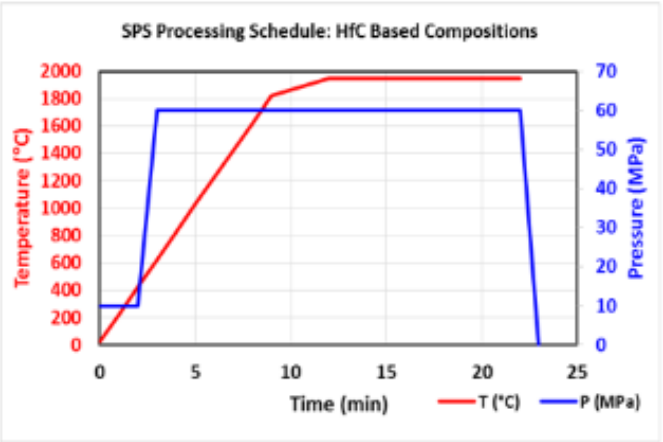

Figure 6: Spark Plasma Sintering template for development of HfC and HfC-SiC Ceramic Composites

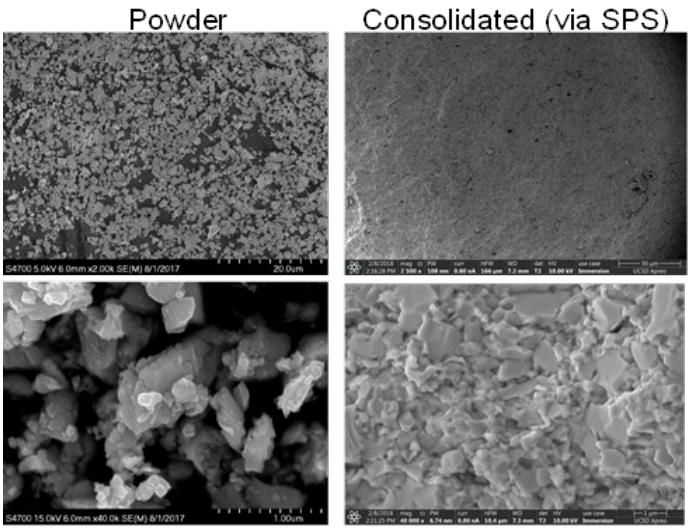

Figure 7: Hafnium Carbide (a) Powder (b) Consolidated using SPS. Lower images are of higher magnification

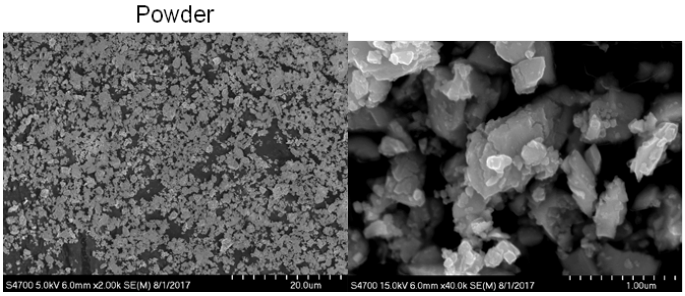

Figure 8: Zirconium Diboride as received powder micrographs

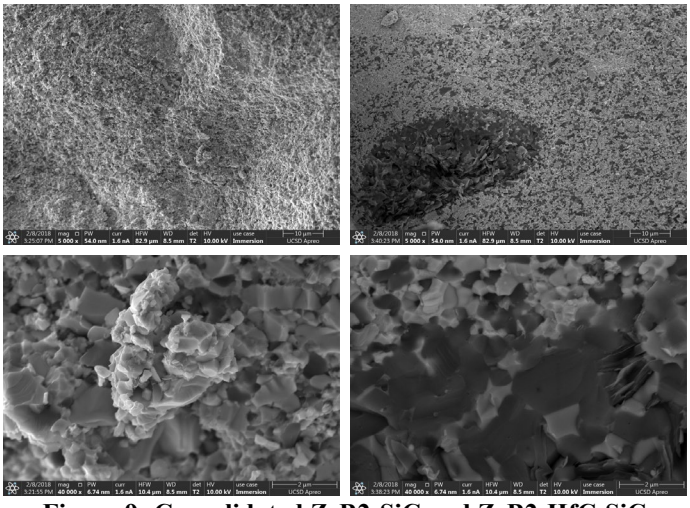

Figure 9: Consolidated ZrB2-SiC and ZrB2-HfC-SiC composites micrographs

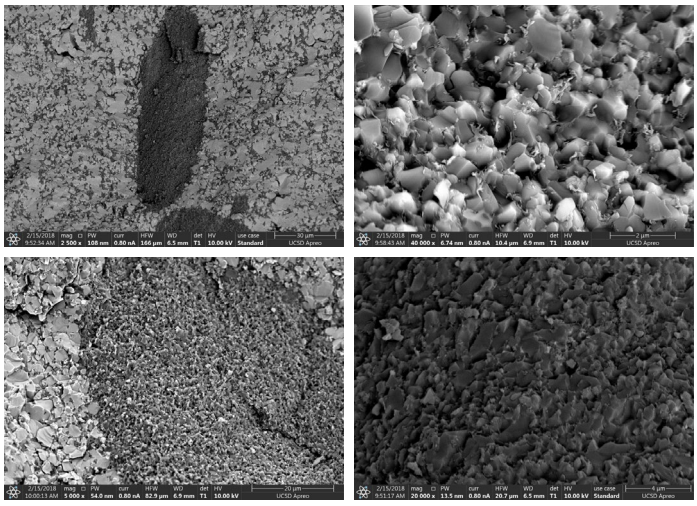

Figure 10: Consolidated HfC-SiC Composite

Ablation Rig Experiments

Each sample underwent ablation testing at a temperature of approximately 2000°C for 10 minutes. Figure 11 shows the ARL Ablation Experimental Test Rig setup and actual experiment in progress. The ASTM E285 ablation testing standard is used as a guide. In the high temperature, ablation experimental test rig, a Harris torch using oxy-propane fuel (neutral flame), is deployed at a standoff distance of 9 millimeters from the sample surface. The temperature is measured using a dual-wavelength (DW) pyrometer while a mid-wave infrared (MWIR) camera produced the temperature profile. These conditions were meant to simulate hypersonic application conditions. Figure 12 shows the samples for both HfC and ZrB_2 based UHTC composites after the 10 minutes of the high temperature testing. Samples were metallographically sectioned, ground using SiC papers, and polished using a 1 µm diamond solution.

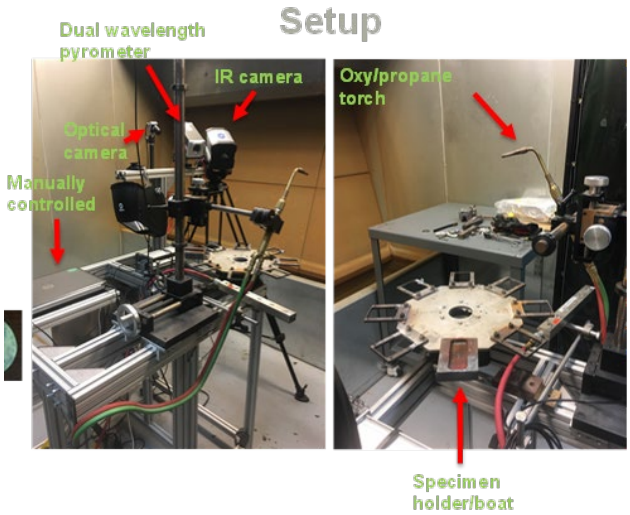

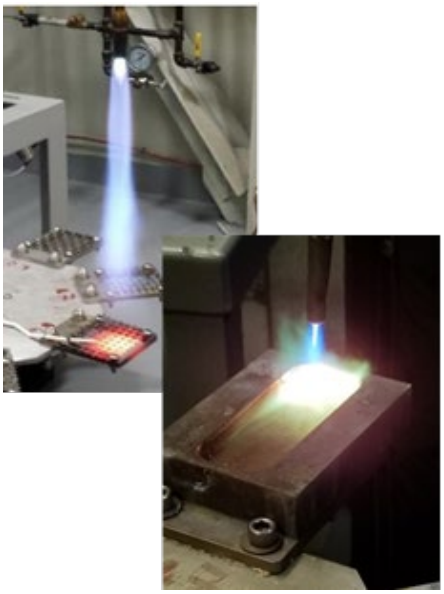

Figure 11: Ablation Flame Experimental Rig Test Setup

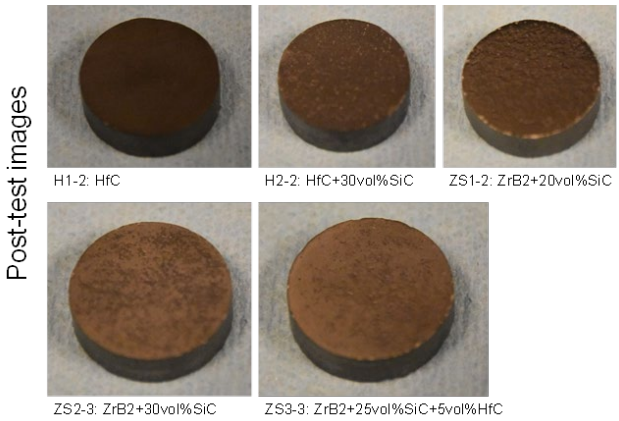

Figure 12: Post-test images of UHTC composite specimens

RESULTS

ZrB_2 UHTC Composites

The sample with the higher SiC content, ZS2, was found to have a thinner ZrO_2 scale and thicker silica glass layer than ZS1, which has the lowest SiC content. This silica glass layer, which is a liquid phase, is beneficial for the prevention of oxidation because it essentially seals the base material [13]. ZS1 had a much thicker protective layer than ZS2 and ZS2's surface was covered with a thick silica-based glass layer which protects the inner material [12]. Figure 12 illustrates scanning electron microscopy of the ZS1 sample which shows thermal stress induced internal cracking and SiC depleted region of ZrB_2 with some ZrO_2 formation. Figure 13 illustrates SEM images of ZS3 sample showing the crystalline of zirconia and boron and in the oxide layer and internal cracking due to thermal stresses. The lightest regions are Zirconium and the darker region are Boron rich, while the circular bubble-like features are SiO_2.

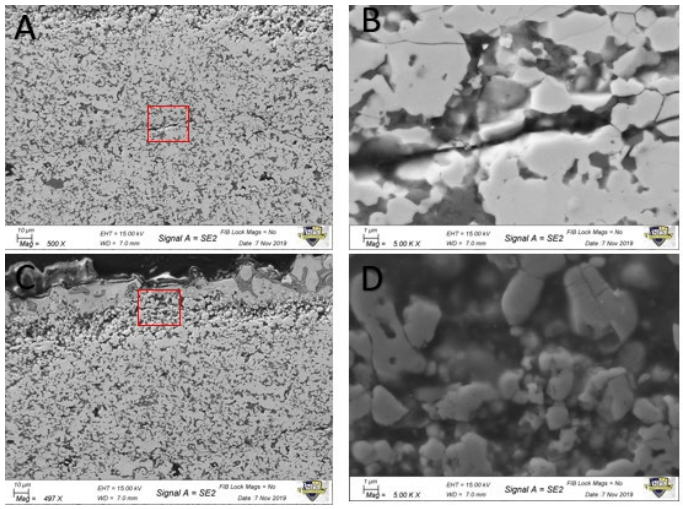

Figure 12: SEM Images of ZSI shows (a-b) an interior, thermal crack, (c-d) porous, SiC depleted region of ZrB2

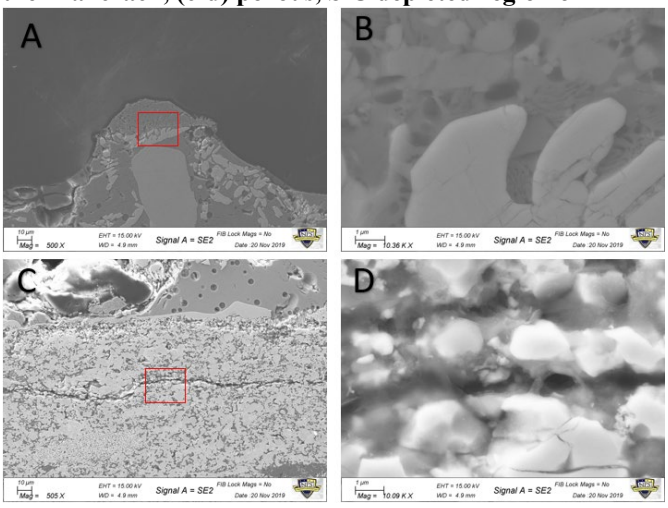

Figure 13: SEM Images of ZS3 (a-b) depicting crystalline structures of zirconia and boron and in the oxide layer (c-d) internal, thermal cracking of the sample.

Mechanical Properties

In order to measure the hardness of the material or its resistance to permanent deformation, nanoindentation testing was performed. The load-displacement curves are shown in Figure 14 for both the bulk material and the near oxide areas. The tabulated values of elastic modulus and nanohardness are provided in Table 2. The highest mechanical properties correspond to the composite with the least amount of SiC phase, ZS2, which contains 20 vol.%. Interestingly, ZS3 has significantly higher mechanical properties than ZS2, though they contain the same amount of ZrB_2 (70 vol.%), ZS3 contains 5 vol.% HfC that appears to enhance mechanical properties in comparison to ZS2 that contains the same amount of ZrB_2, but only SiC (30 vol.%) and no HfC. Differences in nanohardness were more subtle, with ZS2 (lowest SiC content) exhibiting slightly higher values.

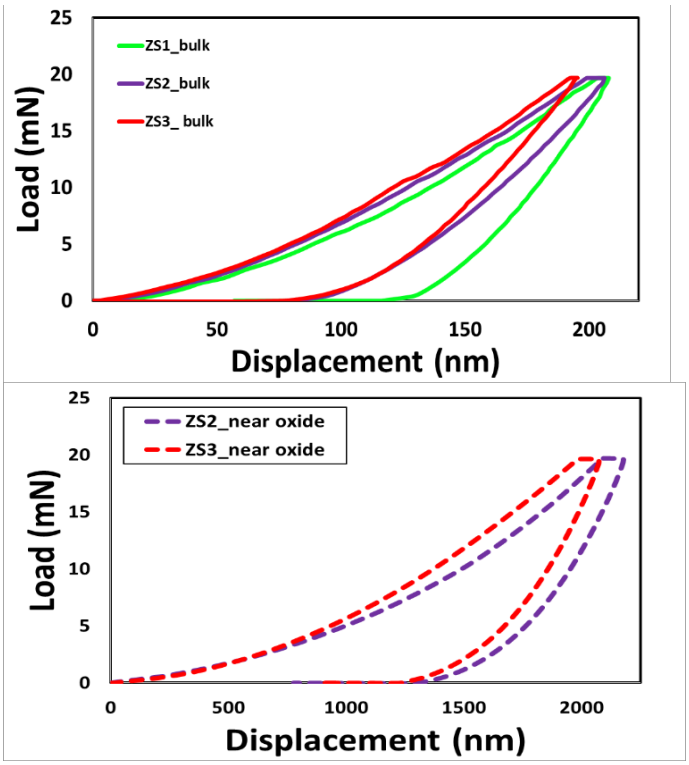

Figure 14: Nanoindentation Load-Displacement Curves; Top: bulk material, Bottom: Near oxide regions on the right image

After the oxidation tests, nanoindentation tests were conducted on the subsurface region nearest the oxidized surface in order to gauge the effect of localized cracks and porosity The values were greatly weakened due to the porous and cracked nature of the oxide and interface region. A loss of strength was expected in the near-surface as significant diffusion from the bulk to the surface occurs during oxide formation. In the near oxide load-displacement graph, ZS2 appears to be relatively softer than ZS3. Once again the incorporation of HfC appears to show some benefit relative to the ZrB_2 composite reinforced with only SiC..

Table 2: Elastic Modulus and Hardness of ZrB2-based UHTCs.

Sample	Elastic Modulus (GPa)	Hardness (GPa)
ZS1	496 ± 72	26 ± 4.1
ZS2	343 ± 60	24 ± 8.4
ZS3	421 ± 83	23 ± 7.6
ZS2 – Near Oxide	4.7 ± 0.1	0.2 ± 0.0
ZS3 – Near Oxide	5.2 ± 0.2	0.2 ± 0.0

Microhardness testing is conducted on both the interior and near-surface regions of each sample, Figure 15.

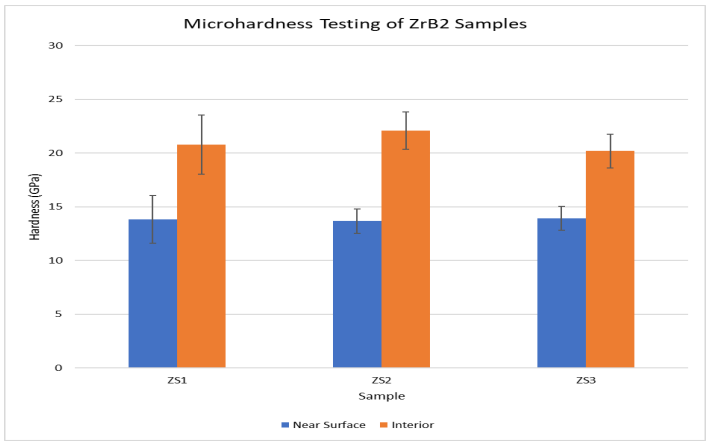

Figure 15: Comparison of the microhardness of each sample's near surface and interior material

In each case, the near-surface area, adjacent to the oxide layer, exhibited a significant decrease in hardness. ZS2 exhibited a 38.2% decrease while ZS1 and ZS3 had similar but slightly less dramatic deterioration with hardness declines of 33.5% and 34.1% respectively. Testing avoided the areas that had long cracks parallel and just interior to the oxide layer. The objective of this test was to gauge overall structural integrity. Each sample showed brittle behavior when the indenter penetrated the material too close to the edge, or oxide region. In these cases, the hardness value could not be collected due to the disfigured, sheared nature of the region.

Hafnium Carbide (HfC) UHTC Composites

For this research the HfC UHTC samples fabricated and tested are HfC and HfC-SiC. Like the ZrB_2 samples the HfC and HfC-SiC samples are fabricated using Spark Plasma Sintering (SPS). The optical microscopic images in Figure 16(a) shows the HfC oxide layer thickness to be 384.0 + 15.2 µm where Figure 16b shows the HfC-SiC oxide layer measured as 1102.2 + 165.3 µm. While SiC is known to enhance oxidation resistance in ZrB_2, in HfC system it may disturb the protective HfO_2 layer. HfC oxide layer is generally uniform as shown in Figure 17, although some significant separation and/or spallation is seen. The oxide is more porous near the surface than the bulk material. For the HfC-SiC the cxide layer is less uniform than HfC oxide layer as shown in Figure 18. Oxide spallation is more prevalent in HfC-SiC. Furthermore, the HfC-SiC composite had pools of SiC that may rapidly oxidize into SiO2 and subsequently volatize as discussed earlier. The coefficient of thermal expansion mismatch of the formed oxide layer with the underlying bulk substrate can also enhance the spallation effect.

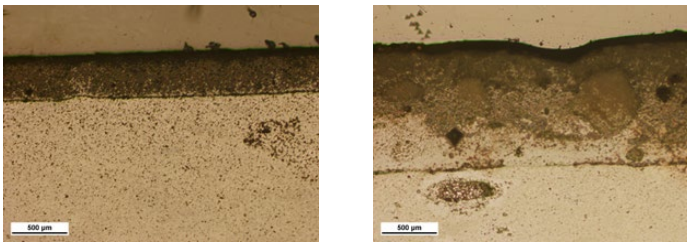

Figure 16: Optical Microscopy showing HFC and HFC-SiC Oxide Layers Thickness Measurement

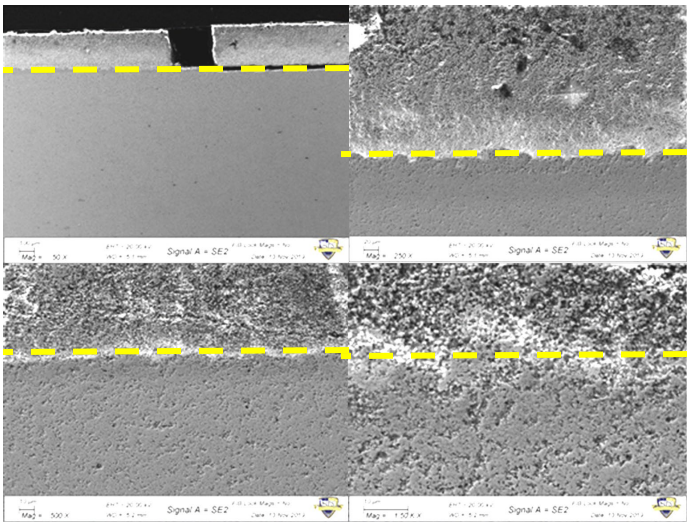

Figure 17: HfC Oxide Layer Boundary

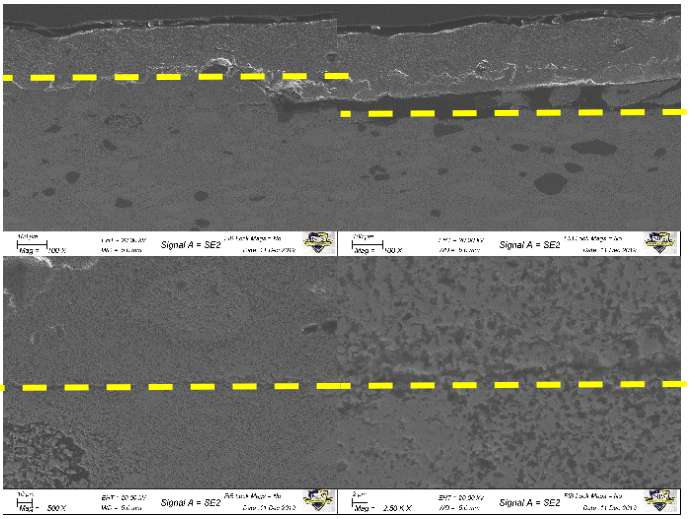

Figure 18: HfC-SiC Oxide Layer Boundary

Nanoindentation Testing

The nanoindentation testing results show that the HfC and HfC-SiC have approximately the same elastic modulus, plasticity, and hardness. The HfC-SiC oxide layers is significantly softer than the oxide layer on HfC, likely because of its porous nature that enables oxide infiltration and more rapid growth of this non-protective oxide. This evaluation is meant to reflect on the structural integrity of the base UHTC and the formed oxide, and as such, oxide values less than those reported in the literature are not surprising given the harsh nature of the test.

Summary of HfC and HfC+SiC UHTC Composites

Introduction of SiC into HfC correlated to the material oxidizing more. HfC-SiC oxide layer is more likely to separate from the bulk material. Load-displacement curves in Figure 19 show that HfC-SiC oxide layer had lower hardness, but exhibited greater plasticity, which could be an advantageous trait if it could be made less permeable to oxygen. The poor performance of HfC-SiC may be largely attributed to the large pools of SiC that would preferentially oxidize and volatize, leaving behind large voids.

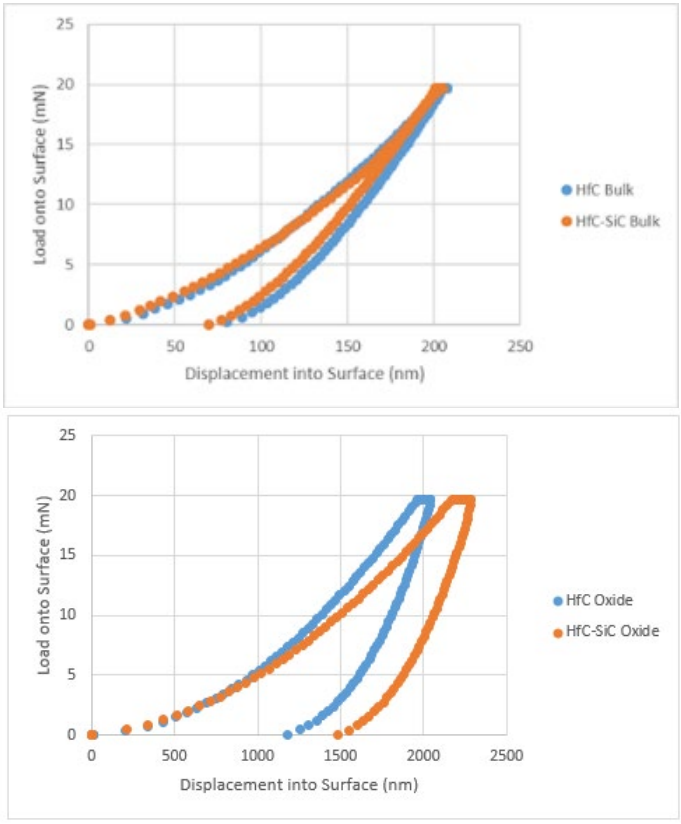

Figure 19: Nanoindentation test results for (a) HfC and (b) HfC-SiC

High Entropy Oxides (HEO) CMAS infiltration Assessment

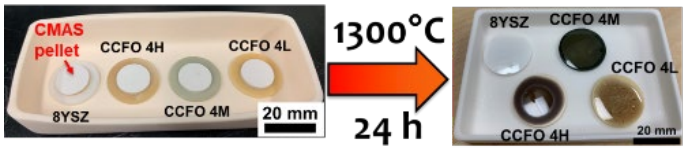

Figure 20: HEO pellets with and without CMAS.

Figure 20 shows the HEO pellets with and without CMAS subjected to isothermal testing at 1300 °C for a duration of 24 hours for the following HEO samples. The chemical compositions of the HEO samples are given below

- 4L – $(Hf_{0.314}Zr_{0.314}Ce_{0.314})(Y_{0.029}Yb_{0.029})O_{2-\delta}$
- 4M – $(Hf_{0.284}Zr_{0.284}Ce_{0.284})(Y_{0.074}Yb_{0.074})O_{2-\delta}$
- 4H – $(Hf_{0.2}Zr_{0.2}Ce_{0.2})(Y_{0.2}Yb_{0.2})O_{2-\delta}$

Figure 21 shows the different CMAS infiltration depths for the three HEO samples and the standard 8YSZ sample subjected to various temperature from 1200-1500 °C. Data is generated by measuring the CMAS infiltration layer and the subsequent reprecipitation of oxides, as observed in Figure 22, for example. HEOs outperform as thermal insulator/barriers at temperature less than 1300 ºC but shows increased reactivity at T > 1300 ºC. Further details of this work is given in Ref [24].

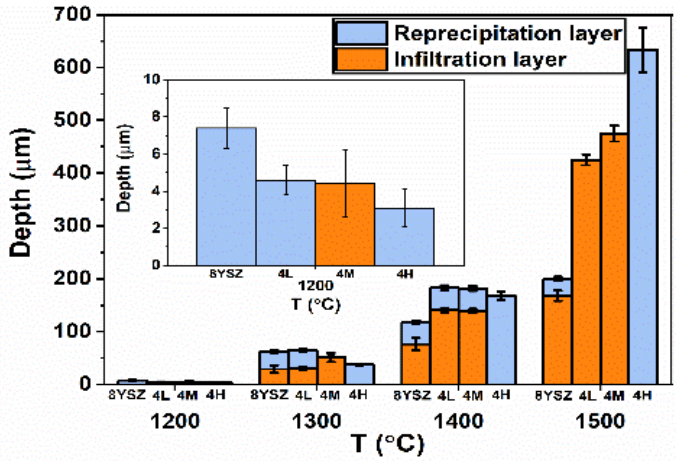

Figure 21: Comparative infiltration measurements of HEO samples with standard 8YSZ Ref [24]

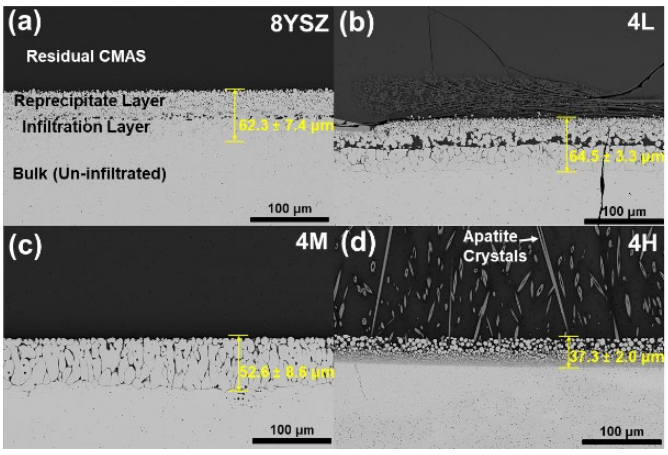

Figure 22: Significant mitigation at "lower" temperatures, but increased reactivity at T > 1300 ºC [Ref 24]

HEO Ablation Flame Test Rig Experiments

The following eleven compositions (4 samples each) of High Entropy Oxides (HEO) are tested at the ARL's Ablation Flame Test Rig for thermal shock and ablative resilience at 2000 °C.

- 3YSZ
- 8YSZ
- HEO4 (B, C, D)
- (Hf, Ce, Zr) (Y, Yb) O2-δ
- HEO5 (B, C, D)
- (Hf, Ce, Zr) (Y, Ca) O2-δ
- HEO7 (B, C, D)
- (Hf, Ce, Zr) (Y, Gd) O2-δ
- B variant: (HfCeZr)0.600 (Stabilizers)0.400 O2-δ (Max configurational entropy)
- C variant: (HfCeZr)0.852 (Stabilizers)0.148 O2-δ (8YSZ-like)
- D variant: (HfCeZr)0.942 (Stabilizers)0.058 O2-δ (3YSZ-like)

The thermal shock and ablation testing is conducted using oxy/propane torch. The distance from flame to sample was 19 mm (from ASTM standard). The flame was held on the surface of the sample for 5 min. The surface T was about 1900 – 2000 °C according to dual wavelength pyrometer. The pellets are loaded into the corner of the sample holders so that the flow field from the flame would not blow it away. Figure 23 shows Pre and post ablation test images of HEO specimens. Pre-ablation test and post ablation SEM images of the surfaces of specimens are shown in the Figure 24 and Figure 25 respectively. Most of the samples ablated away while sample 4B withstood the ablative erosion and thermal shock better than other samples. Figure 26 shows the sample 4B had a splat morphology formation with loose grains surrounding the splats and on the surface. In general the High Entropy Oxide samples did not survive the ablative erosion at 2000 °C.

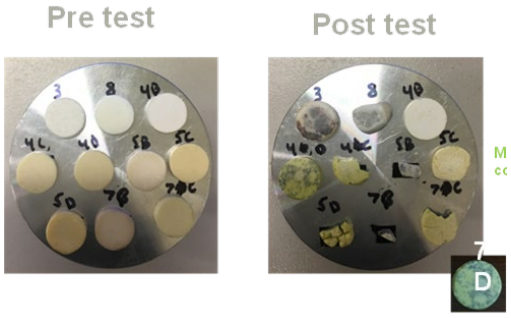

Figure 23: Pre and post ablation test images of HEO specimens

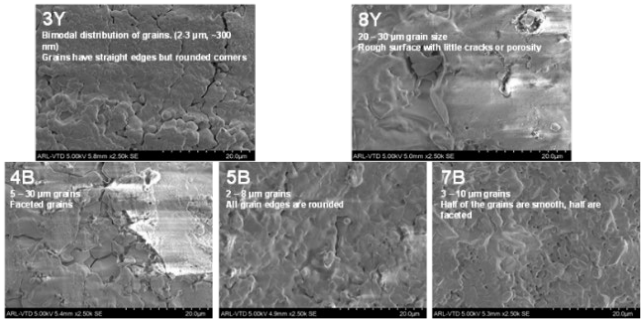

Figure 24: Pre-ablation SEM surface images

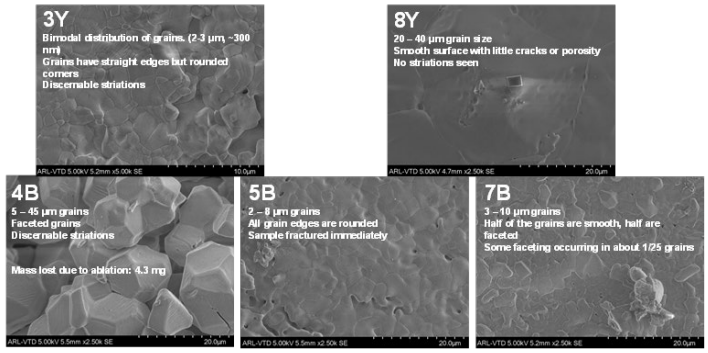

Figure 25. Post ablation SEM surface images

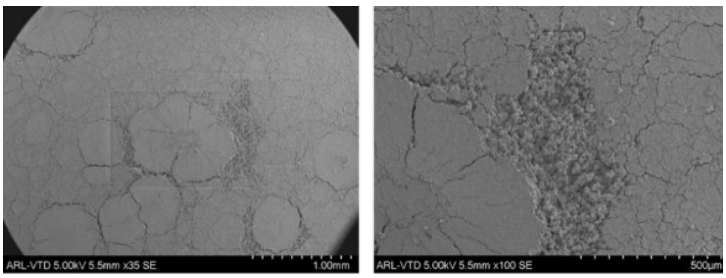

Figure 26: Cracking phenomena observed in sample 4B

High Temperature Thermal Diffusivity of HEO Samples

Sample Prep: Samples are measured for thickness and diameter prior to being coated, on both top and bottom surfaces, with graphite spray. Samples are loaded into a molybdenum sample holder with a fixed diameter of 1cm. Because the software halts the experiment if it cannot make valid measurements on any one sample, samples were run 1 at a time. Each sample is run with a Mo control sample. Thermal diffusivity values for the Mo standard are NIST supplied and used as a check to make sure the machine was working properly. Measurements are to be made from room temperature up to 1000^0C in a nitrogen atmosphere. The software would make the measurements at each temperature until either the last measurement at 1000^0C is completed or no values for diffusivity could be measured. The equipment is programmed to attempt three laser shots on the sample at progressively higher powers if a value cannot be measured or if the attempt at full power fails or if the experiment is halted. 11 out of 13 samples were run. The sample labeled 8Y Standard was not run as the sample was too big for the sample holder. The sample labeled 7C was not run due to a chip falling off from the sample and it as too small for the sample holder.

Mo Control: Due to measurement variability, individual values for the Mo control at each temperature (100, 200 then up to 1600^0C at 200^0C increments) are not provided for the NIST standard. Instead, an acceptable lower limit, center value, and upper limit are provided in units of cm^2/s based on the Clark and Taylor method. The data is considered acceptable as long as the measured value is between the lower and upper limits. As long as the Mo measured control values were within the bounds of the standard, it was assumed that the values for the different samples were also accurate, or at least properly measured. Values for the standard do not exist for measurements at room temperature, however, the limits can be graphed and extrapolated backwards to provide an idea of what would be an acceptable room temperature measurement. For the measurements where the Mo control measured outside of the ranges at either room temperature or 100^0C, the results were still considered valid because the subsequent measurements of the sample were between the lower and upper limits (Figure 27). Overall, the Mo results show that the machine was properly measuring thermal diffusivity during each experiment. The measurements for each point are the average of 3 consecutive shots at each temperature.

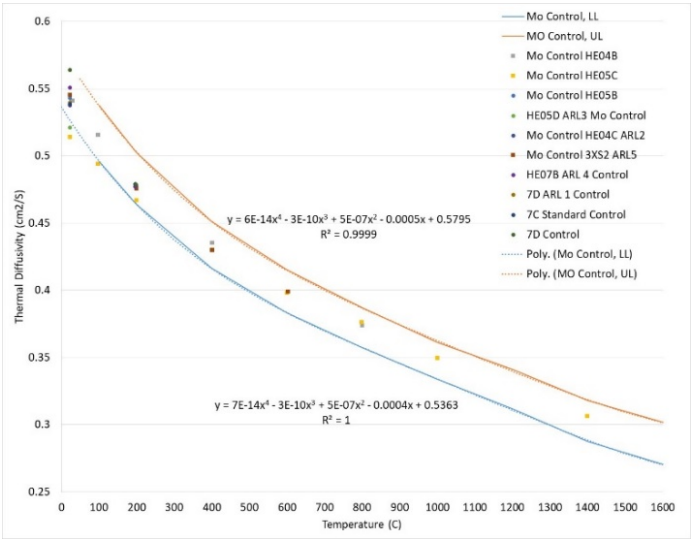

Figure 27. Mo Results

4B: $(Hf_{0.2}Ce_{0.2}Zr_{0.2})(Y_{0.2}Yb_{0.2})O_{1.8}$ 4C: $(Hf_{0.284}Ce_{0.284}Zr_{0.284})(Y_{0.074}Yb_{0.074})O_{1.926}$ 4D: $(Hf_{0.314}Ce_{0.314}Zr_{0.314})(Y_{0.029}Yb_{0.029})O_{1.971}$

5B: $(Hf_{0.2}Ce_{0.2}Zr_{0.2})(Y_{0.2}Ca_{0.2})O_{1.7}$ 5C: $(Hf_{0.284}Ce_{0.284}Zr_{0.284})(Y_{0.074}Ca_{0.074})O_{1.889}$ 5D: $(Hf_{0.314}Ce_{0.314}Zr_{0.314})(Y_{0.029}Ca_{0.029})O_{1.957}$

7B: $(Hf_{0.2}Ce_{0.2}Zr_{0.2})(Y_{0.2}Gd_{0.2})O_{1.8}$ 7C: $(Hf_{0.284}Ce_{0.284}Zr_{0.284})(Y_{0.074}Gd_{0.074})O_{1.926}$ 7D: $(Hf_{0.314}Ce_{0.314}Zr_{0.314})(Y_{0.029}Gd_{0.029})O_{1.971}$

Figure 28. Sample Chemistries

The chemistries for each sample are in Figure 28. The results for HE05C ARL 2 (the orange dots in Figure 29) are incredibly deceptive. Unfortunately for this sample, it is not clear why measurements were repeatedly taken after early results showed

the diffusivity to be 0 from 20 to 800^{0}C; for all other samples, the machine turned off after 1 bad measurement (there are no options in the software to turn this feature off). The increase in thermal diffusivity seen here is driven by the sample reacting with either/both the Mo sample holder and/or the nitrogen atmosphere. After the test, this sample was bonded to the sample holder and had turned black. Sample HE04B ARL2 (the light blue dots) changed colors (from a pale yellow to a darker, more evident, yellow) during testing.

Even when values were measured, they were much less than values measured for Mo. Most of this is due to the ceramic nature of the samples being tested. However, it was observed that often the graphite coating applied to the top surface of the sample would be burned away after testing. While it is most likely that this occurred because of the equipment needed to use higher laser powers to make measurements (making the dissolution of the coating a consequence from extremely low thermal diffusivity), the lack of graphite may have contributed to the extremely low diffusivity values.

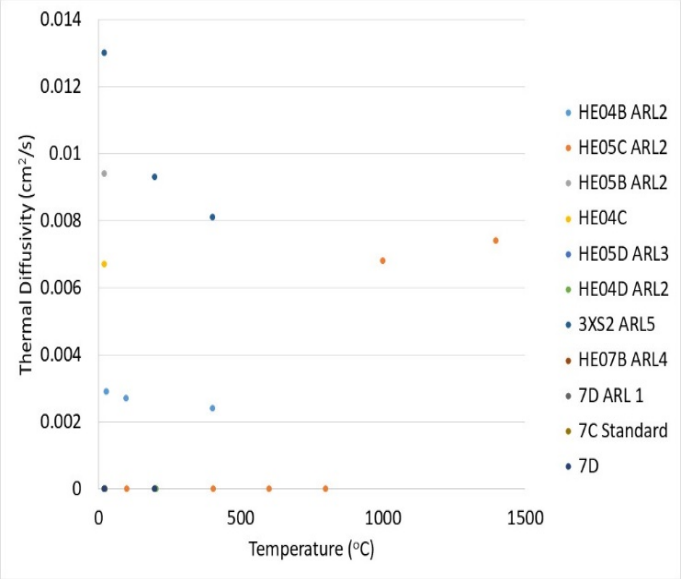

Figure 29. Thermal Diffusivity Results

CONCLUSION AND FUTURE WORK

This paper documents ARL's research in next generation high temperature propulsion material systems which are intended to give our warfighters significant overmatch capability for all weather operability.

- Conventional UHTC compositions need to be further investigated for long temperature thermomechanical durability, oxidation resistance, mechanical properties under engine relevant conditions
  - While introduction of SiC is significant enabler for UHTCs, it lowers the operating temperature of the UHTC composites. Exploratory research on non SiC based UHTC compositions is a significant area.
  - Short continuous UHTCs fiber for fiber reinforced UHTCs needs to be developed
- High-entropy oxides show promise for improved environmental stability, but thermomechanical stability still needs improvement
  - high-entropy borides may be more advantageous route of investigation

ACKNOWLEDGMENTS

This research was supported in part by an appointment to the Postdoctoral Research Participation Program at the U.S. Army Research Laboratory administered by the Oak Ridge Associated Universities through an interagency agreement between the U.S. Department of Energy and DEVCOM ARL. Research was sponsored by the Army Research Laboratory and was accomplished under Cooperative Agreement Number W911NF-16-2-0008. The first author would like to acknowledge the support of DoD Laboratory University Collaborative Initiative (LUCI) Fellowship [2016-2019].

The UHTC specimen fabrication via Spark Plasma Sintering processing was done at UCSD by UCSD and DEVCOM ARL. The ablation experimental testing was conducted at DEVCOM ARL. The microstructure analysis and characterization were performed at NPS. The authors would like to acknowledge the efforts of Mr. Frank Kellogg to conduct the thermal conductivity tests of the oxide specimens.

STANDARD DISCLAIMER

The views and conclusions contained in this paper are those of the authors and should not be interpreted as representing the official policies or positions, either expressed or implied, of the DEVCOM Army Research Laboratory or of the U.S. Government. The U.S. Government is authorized to reproduce and distribute reprints for Government purposes notwithstanding any copyright notation herein.

REFERENCES

1. Ghoshal, A., Murugan, M., Nieto, A., Walock, M. J., Bravo, L., Pepi, M., Swab, J. Hofmeister-Mock, C., Hirsch, S., and Dowding, R.,"High Temperature Ceramic Matrix Composite Materials Research for Next Generation Army Propulsion System, AHS International 74th Annual Forum & Technology Display, Phoenix, Arizona, USA, 2018/5.
2. Walock, M. J., Heng, V., Nieto, A., Ghoshal, A., Murugan, M., and Driemeyer, D. (June 25, 2018). "Ceramic Matrix Composite Materials for Engine Exhaust Systems on Next-Generation Vertical Lift Vehicles." ASME. *J. Eng. Gas Turbines Power*. October 2018; 140(10): 102101. https://doi.org/10.1115/1.4040011
3. Business Insider, Mar 4, 2018, http://www.businessinsider.com/hypersonic-weapons-could-nullify-missile-defenses-2018-2.
4. Johnson, S. M. NASA ARC, UHTC Applications, Issues and Prospects, 2011 http://ceramics.org/wp-content/uploads/2011/08/applicatons-uhtc-johnson.pdf.
5. Wuchina, E, and Opeka, M,, "The Next Step in High Temperature Ceramics," Procs. Engineering Conf International, Ultra High

Temperature Ceramics: Materials for Extreme Environmental Applications II, Spring 5-14-2014.
6. Fahrenholtz, W., Hilmas, G.E, "Ultra-high temperature ceramics: Materials for extreme environments," Scripta Materialia, Volume 129, 2017, Pages 94-99, ISSN 1359-6462, https://doi.org/10.1016/j.scriptamat.2016.10.018. (http://www.sciencedirect.com/science/article/pii/S1359646216305139)
7. Bar-Cohen, Yoseph., "High Temperature Materials and Mechanisms - 6.1 Introduction" (2014).
8. V. Rubio, P. Ramanujam & J. Binner, "Ultra-high temperature ceramic composite, Advances in Applied Ceramics" (2018)
9. Low, I.M., "Advances in Ceramic Matrix Composites - 16.8.1 Self-Healing Protective Coatings at Ultra-High Temperatures" (2014)
10. Gild, Luo et al, "High Entropy Fluorite Oxides," European Ceramic Society Journal, August 2018, https://www.sciencedirect.com/science/article/pii/S0955221918302115.
11. Gild, Luo et al, "High Entropy Metal Diborides" Nature Scientific Reports, 2016. https://www.nature.com/articles/srep37946
12. Rezaie, A., Fahrenholtz, W. G., and Hilmas, G. E., 2006, "Oxidation of Zirconium Diboride-Silicon Carbide at 1500°C at a Low Partial Pressure of Oxygen," Journal of the American Ceramic Society 89 [10] 3240-3245 (2006).
13. Han, J., Hu, P., Zhang, X., and Meng, S., 2007, "Oxidation behavior of zirconium diboride-silicon carbide at 1800°C," Scripta Materialia 57 (2007) 825-828.
14. Zhang, S. C., Hilmas, G. E., and Fahrenholtz, W. G., 2008, "Improved Oxidation Resistance of Zirconium Diboride by Tungsten Carbide Additions," Journal of the American Ceramic Society 91 [11] 3530-3535 (2008).
15. Kubota, Y., Tanaka, H., Arai, Y., Inoue, R., Kogo, Y., and Goto, K., 2017, "Oxidation behavior of ZrB2-SiC-ZrC at 1700°C," Journal of the European Ceramic Society 37 (2017) 1187-1194.
16. Fahrenholtz, W. G., 2007, "Thermodynamic Analysis of ZrB2-SiC Oxidation: Formation of a SiC-Depleted Region," Journal of the American Ceramic Society 90 [1] 143-148 (2007).
17. Gasch, M. J., Ellerby, D. T., and Johnson, S. M., 2005, "Ultra High Temperature Ceramic Composites", Handbook of Ceramic Composites. N. P. Bansal, ed., Springer US, Boston, MA, pp. 197-224.
18. Wu, Z., Wang, Z., Shi, G., and Sheng, J., 2011, "Effect of surface oxidation on thermal shock resistance of the ZrB2-SiC-ZrC ceramic," Composites Science and Technology 71 (2011) 1501-1506.
19. Hong, Q.-J.; van de Walle, A. Prediction of the material with highest known melting point from ab initio molecular dynamics calculations. Phys. Rev. B 2015, 92, 020104.
20. Katoh, Y.; Vasudevamurthy, G.; Nozawa, T.; Snead, L.L. Properties of zirconium carbide for nuclear fuel applications. J. Nucl. Mater. 2013, 441, 718-742. [CrossRef]
21. Charpentier, L., Balat-Pichelin, M., Sciti, D., & Silvestroni, L. (2013). High temperature oxidation of Zr- and Hf-carbides: Influence of matrix and sintering additive. Journal of the European Ceramic Society, 33(15-16), 2867-2878.
22. Young-Hoon Seong, Changyeon Baeka, Joo-Hyung Kim, Jung Hoon Kong, Dong Seok Kim, Sea-Hoon Lee, Do Kyung Kim. (2018). Evaluation of oxidation behaviors of HfC-SiC ultra-high temperature ceramics at above 2500 °C via oxyacetylene torch
23. Ren, J., Zhang, Y., Zhang, P., Li, T., Li, J., & Yang, Y. (2017). Ablation resistance of HfC coating reinforced by HfC nanowires in cyclic ablation environment. Journal of the European Ceramic Society, 37(8), 2759-2768.
24. Wright, AJ, Huang, C, Walock, MJ, Ghoshal, A, Murugan, M, Luo, J. Sand corrosion, thermal expansion, and ablation of medium- and high-entropy compositionally complex fluorite oxides. J Am Ceram Soc. 2020; 104: 448– 462. https://doi.org/10.1111/jace.17448